



Research article

UDC 69

DOI: 10.34910/MCE.137.6



Contact of swivel construction spherical hinge

F. Nie¹, X. Zhou², H. Wang¹ ✉, C. Zhang¹

¹ Dalian University of Technology, Dalian, China

² China Railway 11th Bureau Group Ltd., Wuhan City, China

✉ wanghuili@dlut.edu.cn

Keywords: contact theory, inadequate contact, spherical hinge, swivel construction, unbalanced weight

Abstract. In this paper, the contact stress of the spherical hinge is analyzed. By comparing the finite element model with the calculation results of the related contact theory, it is found that the distribution mode of the contact stress of the spherical hinge is similar to that of the vertical compressive stress distribution model of the spherical hinge, while Hertz contact theory is not suitable for analyzing the contact problem of the spherical hinge. In addition, the existence of unbalanced weight and inadequate contact between the upper and lower spherical hinges are studied in this paper. The results show that for a 30,000-ton swivel bridge, when the unbalanced moment is 0.5×10^4 KN·m~ 2.0×10^4 KN·m, the contact stress in the middle area of the spherical hinge increases, and the contact stress difference between the two sides also increases gradually, up to 16.97 % of the maximum contact stress. When the non-contact area of the middle of the spherical hinge is 10 %, 20 % and 40 %, the maximum contact stress and friction force at the edge of the spherical hinge increase by 9.41 % and 16.16 % respectively compared with the normal situation, but the total friction torque hardly changes.

Funding: This research was funded by the Liaoning Provincial Department of Transportation Foundation Projects (202327).

Citation: Nie, F., Zhou, X., Wang, H., Zhang, C. Contact of swivel construction spherical hinge. Magazine of Civil Engineering. 2025. 18(5). Article no. 13706. DOI: 10.34910/MCE.137.6

1. Introduction

With the rapid development of the transportation industry, the demand for bridge construction in areas with complex terrain and high traffic volumes has been steadily increasing [1]. In particular, when bridges are required to span mountainous regions, deep rivers, or existing transportation corridors, conventional construction methods often face significant limitations. To ensure construction safety and reduce interference with underlying traffic, the swivel construction method has emerged as an effective solution [2–6].

The swivel construction method involves rotating the prefabricated bridge superstructure into its designated position, during which the entire load is transferred through a specialized rotating system. This method has been successfully applied to various bridge types, including beam bridges [7], rigid frame bridges [8], arch bridges [9, 10], and cable-stayed bridges [11–15]. However, during the swivel process, factors such as wind load, unbalanced driving force, and superstructure eccentricity can significantly affect both the dynamic behavior of the bridge and the performance of the rotating system. Ensuring the stability of the rotating process and the mechanical reliability of the swivel components is therefore critical.

Among these components, the spherical hinge plays a pivotal role as the central load-bearing and rotating element. Although the construction technology of the swivel system has become increasingly mature, theoretical research and design guidelines related to the spherical hinge have lagged behind. The calculation method currently prescribed by design standards is overly simplified, often neglecting the

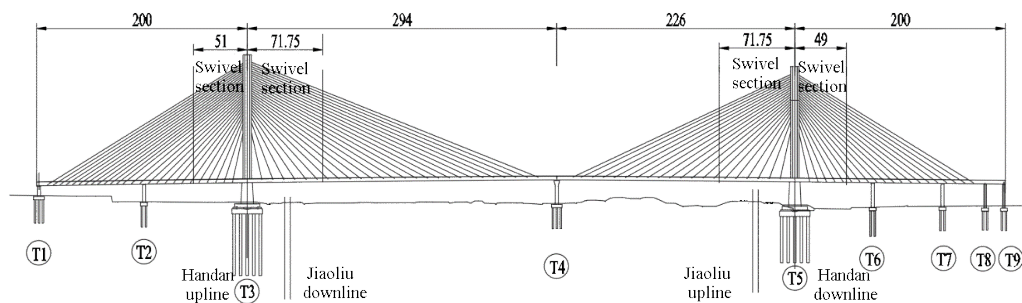
camber-induced stress states and assuming idealized contact conditions. Furthermore, due to the nearly identical radii of curvature and contact areas of the upper and lower spherical components, the assumptions underlying Hertz contact theory—such as small contact areas and dissimilar radii—are not satisfied, limiting its applicability to spherical hinges. These shortcomings have prompted numerous studies focusing on the contact stress, geometric optimization, and design criteria of spherical hinges [16–19]. For example, Feng et al. [10] analyzed radial stress distributions and proposed parameter selection guidelines; Quan et al. [6] introduced design methods for conditions involving unbalanced torque; Zhao [20] examined the mechanical behavior of steel spherical hinges in asymmetrical swivel systems; and Huang et al. [21] refined the calculation method for interface friction.

In light of the above, a more accurate understanding of the contact behavior of spherical hinges is essential for improving design safety and construction reliability. This study investigates the mechanical characteristics of spherical hinges used in the swivel construction of a cable-stayed bridge at the Xiangyang North Railway Yard. Through finite element simulations and theoretical analysis, the distribution pattern of contact stress is compared with classical models, demonstrating that the actual stress distribution more closely aligns with vertical compression patterns rather than the predictions of Hertz theory. The aim is to provide an improved theoretical basis and reference for the design and analysis of spherical hinges in swivel bridge construction.

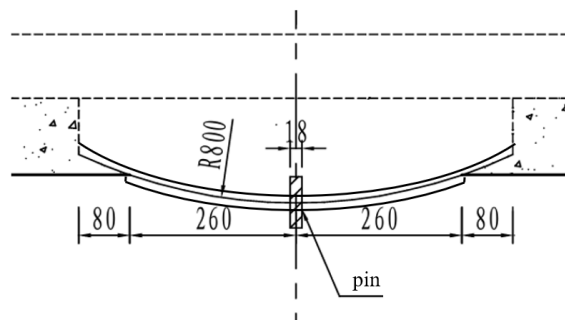
2. Methods

2.1. Project Profile

The bridge across Xiangyang North Railway Marshalling Station is a control joint project of Xiangyang Loop speed improvement project. The bridge is a hybrid girder cable-stayed bridge with double single tower and double cable planes, and the span arrangement is (200 + 294 + 226 + 200) m. Considering that the bridge spans the passenger line, the swivel construction method is used to reduce the impact on the railway line. After the construction of T3 and T5 bridge towers to 73 m above the bridge floor, the bridge began to rotate. The beam length of the swiveling part of T3 bridge tower is 122.75 m, of which the length of the side span concrete part is 51 m, and the length of the main span steel-concrete composite part is 71.75 m. The beam length of the swiveling part of the T5 bridge tower is 120.75 m, of which the length of the side span concrete part is 49 m, and the length of the main span steel-concrete composite part is 71.75 m as shown in Fig. 1a. The total weight of the upper swiveling structure is about 30,000 tons. Fig. 1b shows the elevation of the rotary system. The curvature radius of the spherical hinge is 800 cm, the bearing radius is 260 cm, and the aperture of the pin is 18 cm.



(a) Elevation of bridge structure (unit: m)



(b) Elevation of rotary system (unit: cm)

Figure 1. Structure of bridge across Xiangyang North Marshalling Station.

2.2. Contact Theory

This section will introduce the engineering simplified calculation method and related theory of spherical hinge contact problem.

2.2.1. Engineering simplified algorithm

The simplified algorithm assumes that the contact surface of the upper and lower spherical hinges is a plane, and the contact pressure of the spherical hinge interface is [22]:

$$\sigma = \frac{F}{\pi R^2}, \quad (1)$$

where F is the self-weight load of the superstructure; R is the bearing radius of the spherical hinge.

2.2.2. The normal distribution force on the boundary of the half-space body

Assuming that the uniform normal load q acts on the circular area of radius a , the Poisson's ratio of the spherical hinge material is μ , and the stress at any point on the spherical hinge structure can be solved by the superposition method. For the stress at any point on the z -axis, the contact stress formula of the spherical hinge is [23]:

$$\sigma = \frac{q}{2} \left[(1+2\mu) + \frac{z^3}{(z^2+a^2)^{\frac{3}{2}}} - \frac{2(1+\mu)z}{(z^2+a^2)^{\frac{1}{2}}} \right], \quad (2)$$

when q , a , μ is known, the contact stress of the spherical hinge is only related to z , that is, the above formula represents the distribution law of the contact stress of the spherical hinge.

2.2.3. Vertical compressive stress distribution model of spherical hinge

For the contact surface of the spherical hinge, the vertical compressive stress distribution mode is [24]:

$$p = p_0 \left(1 - \frac{r^2}{a^2} \right)^n, \quad (3)$$

where r is the distance from a point on the contact surface to the contact center; a is the contact radius; p_0 is the vertical stress of the contact center as shown in Fig. 2. When the pressure distribution is the pressure distribution of the Hertzian contact, n is 1/2. When the contact surface produces a uniform normal displacement, n is $-1/2$, then the pressure distribution of the spherical hinge contact can be described [25].

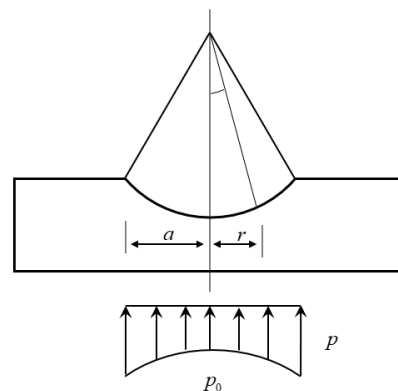


Figure 2. Vertical compressive stress distribution diagram of spherical hinge contact surface.

2.3. Hertz Contact Theory

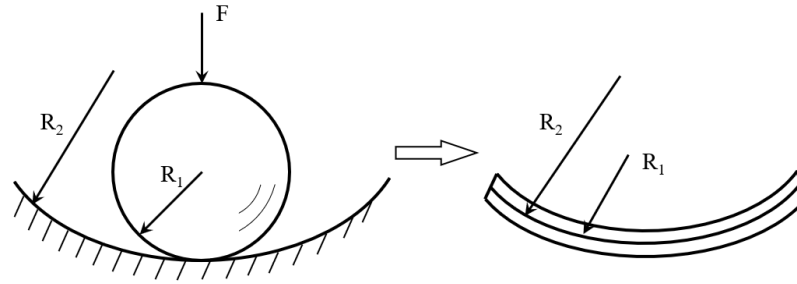


Figure 3. Schematic diagram of Hertz contact model.

Fig. 3 shows a schematic of the Hertzian contact model. In the case of an internal contact between the two spheres, the maximum contact stress of Hertz contact theory can be expressed as [24]:

$$\sigma_{\max} = \frac{1}{\pi} \sqrt[3]{6F \left(\frac{\frac{1}{R_1} - \frac{1}{R_2}}{\frac{1-\mu_1^2}{E_1} + \frac{1-\mu_2^2}{E_2}} \right)}, \quad (4)$$

where F represents the load, R_1 , R_2 represents the radius of curvature of the inner and outer circles; E_1 , E_2 represents the elastic modulus of the inner and outer circles; μ_1 , μ_2 represents the Poisson's ratio of the inner and outer circles. When $E_1 = E_2$, $\mu_1 = \mu_2 = 0.3$, the maximum contact stress is simplified as:

$$\sigma_{\max} = 0.3883 \sqrt[3]{\frac{FE^2 (R_1 - R_2)^2}{R_1^2 R_2^2}}. \quad (5)$$

2.4. Numerical Methods for Contact Problems

At present, the finite element method is widely used in highly nonlinear problems and highly nonlinear contact problems. In this project, the simulation of the contact of the spherical hinge is highly nonlinear contact problems. Therefore, this study will use the finite element method to analyze the spherical hinge contact problem. The contact problem is characterized by the dynamic change of the contact surface, which will lead to the constant change of the constraint conditions in the contact process. Therefore, the incremental method is often used to deal with the contact problem. The contact constraints of the contact problem in the bonded or sliding state can be expressed by the following formula [21, 26, 27]:

$$\begin{cases} u_N^A - u_N^B + g_N = 0 \\ u_T^A - u_T^B = 0 (\text{bond}) \\ |{}^{t+\Delta t} F_T^A| - \mu |{}^{t+\Delta t} F_N^A| = 0 (\text{slide}) \end{cases}, \quad (6)$$

where u_N^A , u_N^B are the normal displacement increments of contact A and B , respectively; g_N is the distance between contact points; u_T^A , u_T^B are the tangential displacement increments of contact A and B , respectively. F_T^A , F_N^A are the tangential and normal forces of the contact body A , respectively. The virtual work equation of the incremental method contact problem based on Lagrange scheme is [21, 26, 27]:

$$\sum_{r=1}^{A,B} \left[\int_{t+\Delta t_{V,r}} {}^{t+\Delta t} \tau_{ij}^r \delta_{t+\Delta t} e_{ij}^{t+\Delta t} dV \right] + \sum_{r=1}^{A,B} \left[\int_{t+\Delta t_{S_G^r}} {}^{t+\Delta t} T_i^r \delta u_i^{t+\Delta t} dS \right] + \int_{t+\Delta t_{S_c}} {}^{t+\Delta t} F_J^A \left(\delta u_J^A - \delta u_J^B \right)^{t+\Delta t} dS = 0, \quad (7)$$

where J is the two vertical directions of the contact surface, $J = 1, 2$. The left superscript of the tensor $t + \Delta t$ is the incremental step expressed in time. The first term of the equation is the virtual strain energy, the second term is the external virtual work generated by the surface force, and the third term is the virtual work generated by the contact force on the contact surface.

The Lagrange multiplier method is introduced to consider the additional constraints. The variation of the displacement increment by the corresponding modified functional is as follows [21, 26, 27]:

$$\sum_{r=1}^{A,B} \left[\int_{t+\Delta t_{V,r}} {}^{t+\Delta t} \tau_{ij}^r \delta_{t+\Delta t} e_{ij}^{t+\Delta t} dV \right] + \sum_{r=1}^{A,B} \left[\int_{t+\Delta t_{S_G^r}} {}^{t+\Delta t} T_i^r \delta u_i^{t+\Delta t} dS \right] + \int_{t+\Delta t_{S_c}} {}^{t+\Delta t} \lambda_J^A \left(\delta u_J^A - \delta u_J^B \right)^{t+\Delta t} dS = 0. \quad (8)$$

In the formula, the first term is the virtual strain energy, the second term is the external virtual work generated by the surface force, and the third term is the virtual work generated by the constrained variable λ (Lagrange multiplier variable).

The whole region is discretized, and the node displacement is used as the basic variable of the shape function. The final finite element solution equation is as follows [21, 26, 27]:

$$\begin{bmatrix} {}^t_0 K_L + {}^t_0 K_{NL} & K_{c\lambda} \\ K_{c\lambda}^T & 0 \end{bmatrix} \begin{pmatrix} u \\ {}^{t+\Delta t} \lambda \end{pmatrix} = \begin{pmatrix} {}^{t+\Delta t} Q_L - {}^t_0 F \\ -{}^t \bar{g} \end{pmatrix}, \quad (9)$$

where K_L is the linear term of the global stiffness of the contact; K_{NL} is the nonlinear term; $K_{c\lambda}$ is the interface constraint stiffness; Q_L is the equivalent nodal load vector.

The first term of matrix (9) is essentially a discrete form of (8). The second term is the discretization form of constraint condition (6). It can be seen from equations (6)–(9) that before solving the contact equation, it is first necessary to determine whether the shortest distance between the two contact points after discretization meets the contact constraint conditions. By adjusting the coordinates of contacts A and B in each incremental step, the new contact point position is obtained, and then calculated according to equation (6). Based on the above theory, the finite element method can simulate the contact problem. The comparison between the simulation results and the theoretical calculation results will be introduced in the next section.

3. Results and Discussion

3.1. Contact Model Comparison

In this paper, ABAQUS finite element analysis software is used to analyze the contact of spherical hinges. Fig. 4 is the schematic diagram of the spherical hinge contact model. The spherical hinge contact model includes a turntable, an upper spherical hinge, a lower spherical hinge, and a foundation slab. The turntable circle and the upper spherical hinge, the foundation slab and the lower spherical hinge adopt tie constraint, while the upper and lower spherical hinges are set as surface to surface constraint, the normal behavior is set to "hard contact", the tangential behavior is set to friction, and the friction coefficient is 0.024 according to the test. The boundary condition is the solid connection between the foundation slab and the ground, and the weight of the superstructure acts on the upper turntable in the form of pressure. All components are finely meshed to ensure a structured grid. All solid components adopt the 3-degree of freedom 8-node element to ensure solution accuracy.

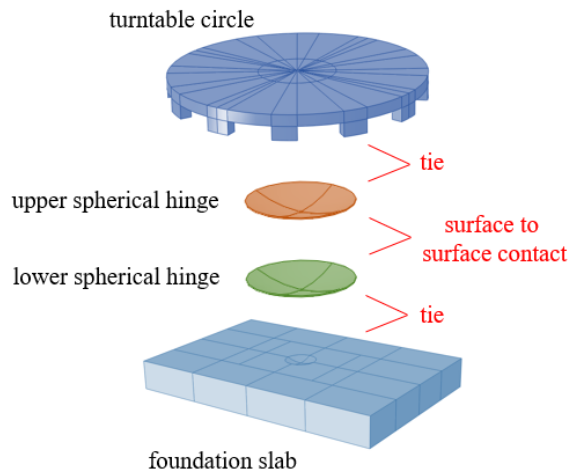


Figure 4. Schematic diagram of spherical hinge contact model.

The contact stress cloud diagram of the spherical hinge during the swivel process is shown in the Fig. 5. The distribution law of the contact stress is gradually increasing from the center of the spherical hinge to the outside. The center contact stress is almost 0 MPa, and the edge contact stress is 58.64 MPa. The contact theory introduced in Section 3 is applied to this problem, and a series of theoretical solutions are listed in the Table 1. The radial distribution of contact stress along the spherical hinge is shown in the Fig. 6. According to equation (1), the contact stress of the spherical hinge obtained by the simplified engineering algorithm is 14.21 MPa, which is no change along the path of the spherical hinge. According to equation (2), the maximum contact stress calculated by the normal distribution force on the boundary of the half-space body is 11.10 MPa. The calculation results of these two methods are quite different from the maximum contact stress obtained by simulation. According to the calculation result of equation (3), it can be seen that the vertical compressive stress distribution model of the spherical hinge is close to the finite element results in the distribution law. According to equation (4), since the curvature radius of the spherical hinge is the same, the maximum contact stress of the Hertz contact theory is 0.

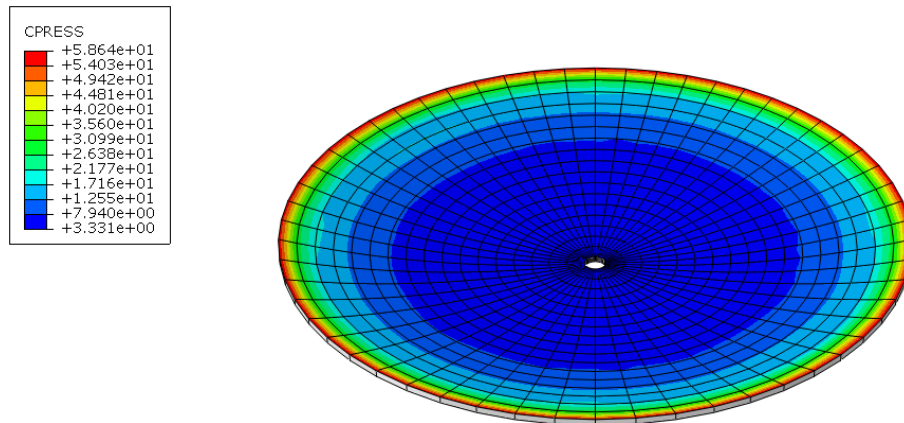


Figure 5. Spherical hinge contact stress cloud diagram.

Table 1 Comparison of finite element and theoretical calculation results.

Theory/algorithmic model	Distance from center of spherical hinge						
	200	600	1000	1400	1800	2200	2580
3.1	14.21	14.21	14.21	14.21	14.21	14.21	14.21
3.2	8.17	8.30	8.57	8.97	9.52	10.23	11.10
3.3	7.13	7.30	7.70	8.43	9.85	11.12	57.39
3.4	0	0	0	0	0	0	0
Finite element method	4.50	5.11	5.53	7.19	8.96	14.07	58.19

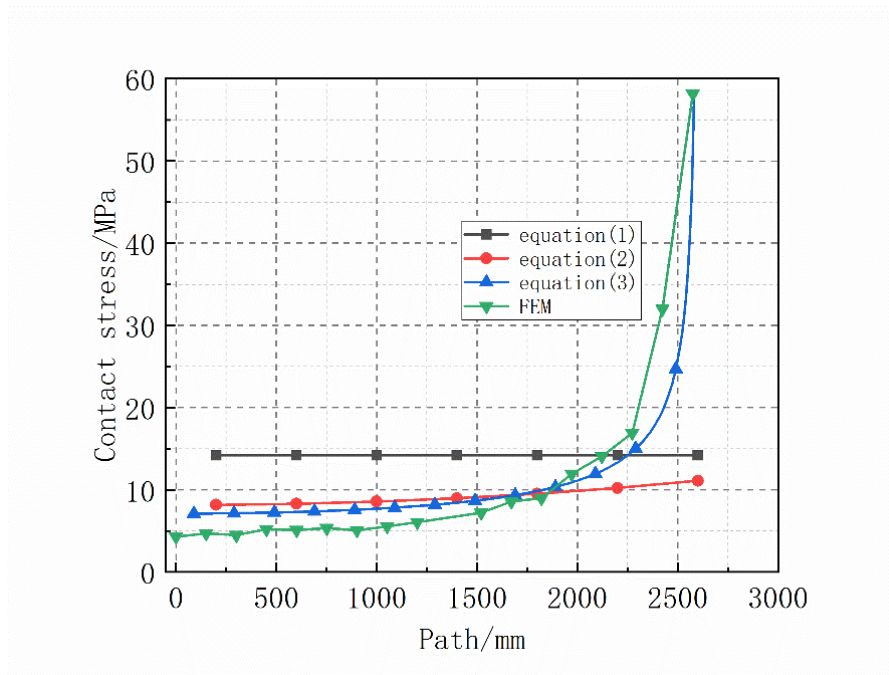


Figure 6. Comparison of contact stress under different calculation methods.

The calculation results of equation (3) show that the contact stress increases rapidly at the edge of the spherical hinge, which is close to the finite element results. In the range of 2000 mm from the center of the spherical hinge, the contact stress calculated by equation (3) is greater than the result of finite element simulation, but it is very consistent with equation (2). In summary, it can be considered that equation (3) is suitable for simulating the contact stress of spherical hinges. For the spherical hinge contact model, the radius of curvature of the inner and outer circles is infinitely close, and the contact stress calculated by Hertz theory is almost zero, which is inconsistent with the actual situation. Therefore, Hertzian contact theory is not suitable for analyzing spherical hinge contact.

In practical engineering, the superstructure and substructure of the swiveling system are connected only through the free contact surface between the upper and lower spherical hinges, and the normal operation of the spherical hinges is the key to ensure the safety of the swiveling process of the bridge. Various influencing factors may lead to the destruction or abnormal operation of the spherical hinge, which in turn leads to the overturning of the bridge during the swivel process. Therefore, this section analyzes the parameters of two kinds of common problems in rotary construction, namely unbalance weight and inadequate contact of spherical hinges.

3.2. Influence of unbalanced weight on spherical hinge

In the process of swivel, the bridge is affected by the uncertain factors such as wind load and temperature action, which will produce additional unbalance torque and cause the risk of overturning. This section explores the influence of unbalance weight on the spherical hinge, and sets five unbalance moments, respectively 0 , 0.5×10^4 KN·m, 1.0×10^4 KN·m, 1.5×10^4 KN·m, and 2.0×10^4 KN·m, which accounts for 0 %, 1.67 %, 3.33 %, 5.00 %, and 6.67 % of the total weight, when the moment arm is taken 1 m. The five conditions are defined as load case I, load case II, load case III, load case IV, and load case V.

Fig. 7 is the schematic diagram of the spherical hinge data extraction path. Fig. 8 shows the spatial displacement curve on the spherical hinge path. With the increase of unbalanced moment, the position 2000 mm away from the center of the spherical hinge becomes the largest part of the vertical displacement of the whole spherical hinge, and the vertical displacement is -0.843 mm, -0.856 mm, -0.870 mm, -0.883 mm, respectively. Through the displacement cloud diagram and displacement curve of the spherical hinge, it can be seen that the existence of unbalanced moment leads to the dislocation between the upper and lower spherical hinges, and as the unbalanced moment increases, the deviation between the two spherical hinges increases.

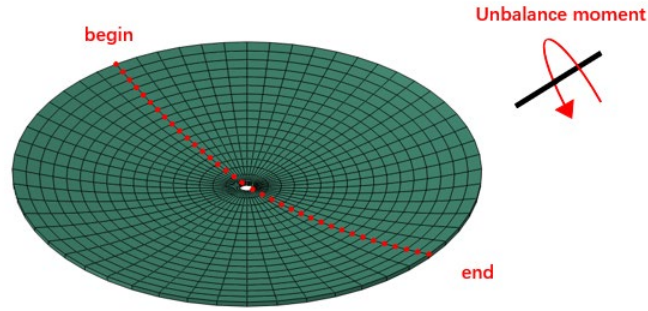


Figure 7. The schematic diagram of the spherical hinge data extraction path.

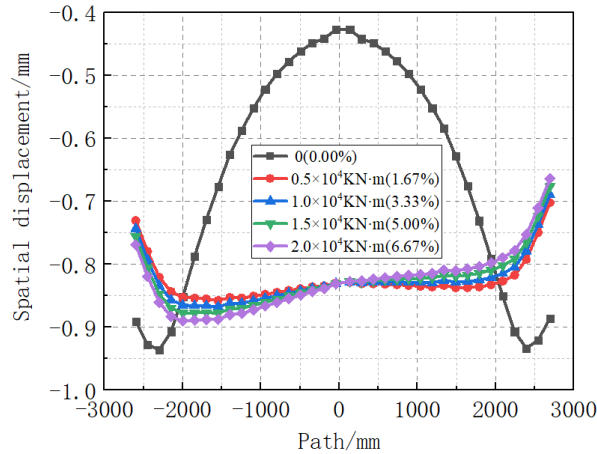


Figure 8. the spatial displacement curve on the spherical hinge path.

Fig. 9a is the contact stress distribution curve on the spherical hinge path. Fig. 9b shows the difference between the contact stress of each point on the path and load case I under five load cases. When there is no unbalanced moment, the contact stress curve is symmetrical about the center of the spherical hinge, and the maximum contact stress is 58.19 MPa. When there is an unbalanced moment, the maximum contact stress at the edge of the spherical hinge decreases, but the contact stress within 2000 mm from the center of the spherical hinge increases. This occurs because when the upper and lower spherical hinges are misaligned, the edge of the spherical hinge becomes suspended, resulting in a decrease in stress. Conversely, the middle contact area diminishes, leading to an increase in contact stress. In addition, the contact stress curve of the spherical hinge with unbalanced moment is no longer symmetrical about the center of the spherical hinge, and with the increase of unbalanced moment, the contact stress difference between the two sides of the spherical hinge increases, reaching 1.05 MPa, 3.89 MPa, 5.71 MPa, and 7.56 MPa, which accounts for 2.51 %, 9.11 %, 13.09 %, and 16.97 % of the maximum contact stress.

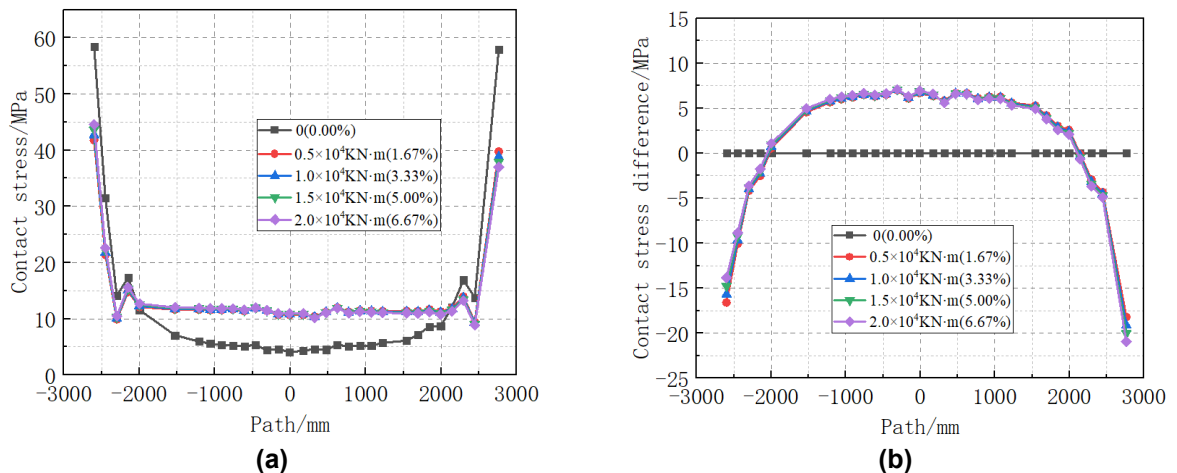


Figure 9. Contact stress (a) and contact stress difference (b) of spherical hinge path under different load case.

3.3. Influence of Inadequate Contact on Spherical Hinge

Inadequate contact between the spherical hinges will change the contact state, thus affecting the force of the spherical hinge. This section explores the impact of inadequate contact on spherical hinges by setting different contact areas for the upper and lower spherical hinges, that is, slightly changing the curvature of the upper spherical hinges, so that some areas of the upper and lower spherical hinges do not have contact. As shown in Fig. 10, four contact conditions are set respectively, which are defined as load cases I, II, III, and IV. Load case I is that the upper and lower spherical hinges have the same curvature and are in complete contact. Load case II to load case IV is that the middle part of the spherical hinges is suspended without contact. The uncontacted part accounts for 10%, 20%, and 40% of the total area of the spherical hinge, respectively.

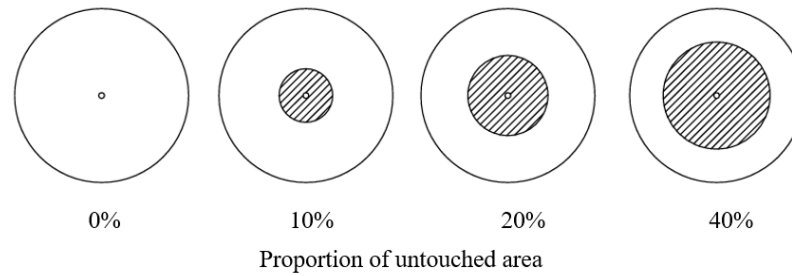


Figure 10. Contact diagram of the spherical hinge (Shadows represent untouched parts).

Fig. 11a is the contact stress curve of the spherical hinge path, and Fig. 11b is the contact stress difference of spherical hinge path. It can be seen that with the decrease of the center contact area, the maximum contact stress on the edge of the spherical hinge gradually increases. However, due to the small contact stress in the middle of the spherical hinge, the inadequate contact of this part has little effect on the overall force of the spherical hinge, so the contact stress distribution of the spherical hinge is almost unchanged. The maximum edge contact stress of load case I to load case IV is 58.64 MPa, 59.94 MPa, 61.90 MPa, and 64.06 MPa, which increases by 2.21%, 5.56%, and 9.41%, respectively, compared with load case I. The growth rate of contact stress shows a gradually increasing trend.

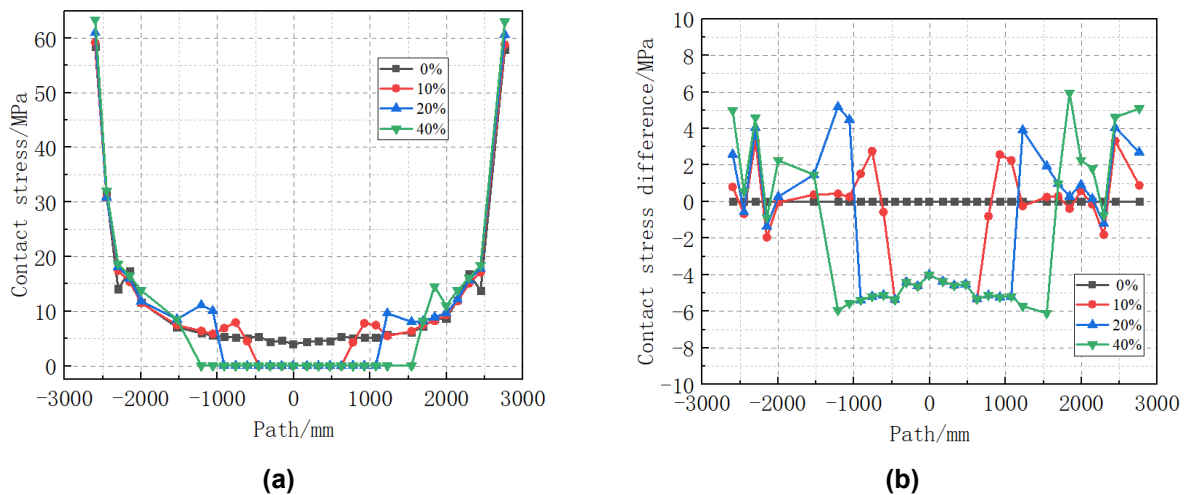


Figure 11. Contact stress (a) and contact stress difference (b) of spherical hinge path under different contact area.

Fig. 12a is the friction curve of spherical hinge path, and Fig. 12b is the friction force difference of spherical hinge path. Similar to the contact stress, the distribution of friction force also shows the law of large edge and gradually decreasing toward the center. The edge friction of spherical hinge under load case I to load case IV is 28.46 kN, 30.22 kN, 31.87 kN, and 33.06 kN, which increase by 6.18%, 11.98%, and 16.16%, respectively, compared with load case I. The frictional resistance moments extracted by ABAQUS during the rotation of the spherical hinge are all 5.8×10^3 kN·m, so the total tractive force required for the rotation of the spherical hinge will not change.

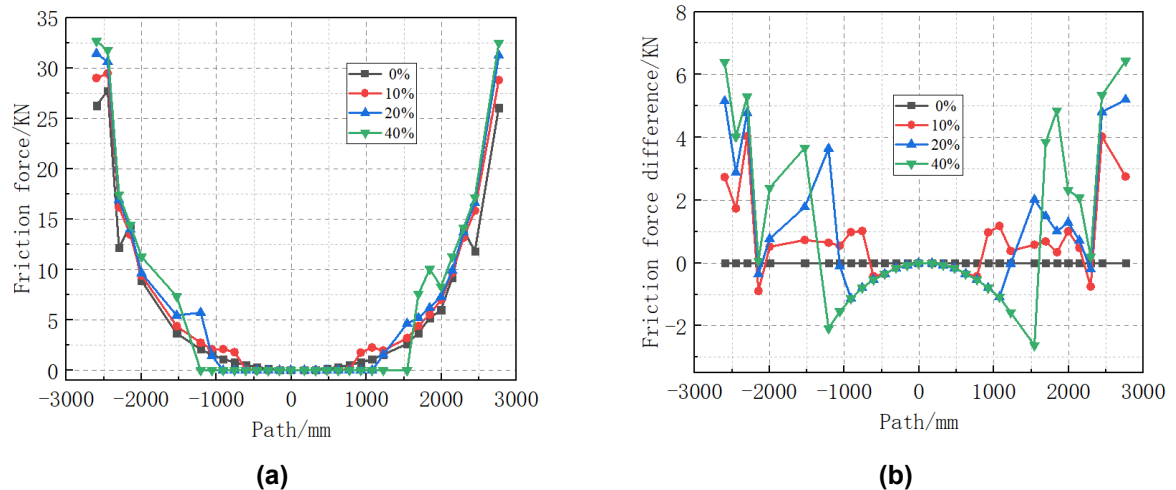


Figure 12. Friction force (a) and friction force difference (b) of spherical hinge path under different contact area.

4. Conclusion

Based on the swivel construction project of the bridge across Xiangyang North Railway Marshalling Station, this paper analyzes the swivel system, especially the spherical hinge, and compares the contact stress of finite element simulation and the results of various spherical hinge contact theory calculations. In addition, this paper also analyzes the response of the spherical hinge under the action of unbalanced moment, and the internal force change of the spherical hinge when the upper and lower spherical hinges are not fully contacted. The conclusions are as follows:

1. The contact stress distribution of the spherical hinge obtained by the finite element simulation is similar to the distribution law of the vertical compressive stress distribution model. In the contact problem of the spherical hinge, the curvature radius of the upper spherical hinge and the lower spherical hinge is almost the same. The contact stress calculated by the Hertz contact theory is 0, so the Hertz contact theory cannot be applied to the calculation of the contact of the spherical hinge.
2. The unbalanced moment will lead to the offset of the upper and lower spherical hinges, and the contact stress distribution of the spherical hinge is not symmetrical about the center of the spherical hinge. Under the same conditions, the contact stress of the edge of the spherical hinge without unbalanced moment is greater, and the contact stress of the middle part of the spherical hinge with unbalanced moment is greater. For a 30,000 ton rotary bridge, when the unbalanced moment is 0.5×10^4 KN·m (1.67 %), 1.0×10^4 KN·m (3.33 %), 1.5×10^4 KN·m (5.00 %), and 2.0×10^4 KN·m (6.67 %), the contact stress difference between the two edges of the spherical hinge reaches 1.05 MPa, 3.89 MPa, 5.71 MPa, and 7.56 MPa, which accounts for 2.51 %, 9.11 %, 13.09 %, and 16.97 % of the maximum contact stress.
3. The inadequate contact between the upper and lower spherical hinges will lead to the increase of the maximum contact stress and the maximum friction force at the edge of the spherical hinge. When the non-contact area of the spherical hinge is 10 %, 20 %, and 40 %, the maximum contact stress of the spherical hinge edge increases by 2.21 %, 5.56 %, and 9.41 %, and the friction force of the spherical hinge edge increases by 6.18 %, 11.98 %, and 16.16 %, respectively, while the total frictional moment hardly changes.

References

1. Zhou, X.H., Zhang, X.G. Thoughts on the Development of Bridge Technology in China. *Engineering*. 2019. 5(6). Pp. 1120–1130. DOI: 10.1016/j.eng.2019.10.001
2. Li, W.-W., Zhang, Z., Huang, C.-L. Application of Dynamic Unstressed State Method in Vertical Rotation Construction of Bridges. *Advanced Materials Research*. 255–260. Pp. 988–992. DOI: 10.4028/www.scientific.net/amr.255-260.988
3. Jia, F.X., Chen, D.W., Wu, Y.Y. Fine-Analysis for the Concrete Upper Rotation Table and Pier of a Bridge Using Rotation Construction Method. *Applied Mechanics and Materials*. 2014. 638–640. Pp. 1099–1102. DOI: 10.4028/www.scientific.net/amm.638-640.1099
4. Su, M., Wang, J., Peng, H., Cai, C.S., Dai, G. State-of-the-art review of the development and application of bridge rotation construction methods in China. *Science China-Technological Sciences*. 2021. 64(6). Pp. 1137–1152. DOI: 10.1007/s11431-020-1704-1
5. Shao, J., Duan, M., Yang, W., Li, Y. Research on the critical technique of synchronous rotation construction with large angle for T-shape curve rigid frame bridge. *Scientific Reports*. 2022. 12. Article no. 1530. DOI: 10.1038/s41598-022-05403-8

6. Quan, W., Zhang, Z., Liu, X., Deng, X. Research on Rotational Spherical Hinge Design Method Considering Unbalanced Moments. *Bridge Construction*. 2023. 53. Pp. 112–119.
7. Siwowski, T., Wysocki, A. Horizontal Rotation via Floatation as an Accelerated Bridge Construction for Long-Span Footbridge Erection: Case Study. *Journal of Bridge Engineering*. 2015. 20(4). Article no. 05014014. DOI: 10.1061/(ASCE)BE.1943-5592.0000693
8. Jiang, L., Gao, R. Deformation monitoring during removal of the supporting of T-type rigid frame bridge constructed by rotation method. *Procedia Engineering*. 2010. 4. Pp. 355–360. DOI: 10.1016/j.proeng.2010.08.041
9. Huang, W. Construction Techniques for Horizontal Rotation of 113-m Span Simply-Supported Tied Arch Bridge on Tianjin Qinhuangdao Passenger Dedicated Railway. *Bridge Construction*. 2012. 42. Pp. 114–120.
10. Feng, Y., Qi, J., Wang, J., Zhang, W., Zhang, Q. Rotation construction of heavy swivel arch bridge for high-speed railway, *Structures*. 2020. 26. Pp. 755–764. DOI: 10.1016/j.istruc.2020.04.052
11. Sun, Q.S., Guo, X.G., Zhang, D.P., Guan, X.K., Zheng, Y. Research on the Application of Horizontal Rotation Construction Method with Flat Hinge in Cable-Stayed Bridge Construction. *Advanced Materials Research*. 2011. 255–260. Pp. 856–860. DOI: 10.4028/www.scientific.net/AMR.255-260.856
12. Wang, S.J., Zhu, X., Gao, Z.D. Research and Application of Level Rotational Construction Technology of DWT Cable-Stayed Bridge. *Advanced Materials Research*. 2011. 163–167. Pp. 2262–2266. DOI: 10.4028/www.scientific.net/AMR.163-167.2262
13. Xiao, J.H., Liu, M., Zhong, T.Y., Fu, G.Z. *IOP Conference Series: Earth and Environmental Science*. 218. Article no. 012087. DOI: 10.1088/1755-1315/218/1/012087
14. Liu, Y. Design of a Rotation-Constructed Cable-Stayed Bridge Carrying Part of Xi'an Ring Expressway over Xi'an North Railway Station. *Bridge Construction*. 2023. 53. Pp. 108–113.
15. Wang, D., Liu, Z., Gao, J., Li, C., Guo, T. Swivel Construction of a Cable-Stayed Bridge for Minimal Disturbance to Adjacent Railways. *Structural Engineering International*. 2023. 33. Pp. 498–505. DOI: 10.1080/10168664.2022.2135165
16. Guo, W., Yu, H., Li, Y., Tian, W., Chen, W. Mechanical characteristics and design parameter analysis of spherical hinge structure for swivel bridge. *Scientific Reports*. 2024. 14. Article no. 29922. DOI: 10.1038/s41598-024-81320-2
17. Wu, H., Yang, Z., Lu, C., Li, Z., Guo, C., Sha, G. The Influence of Key Dimensions of the Swivel Hinge on the Mechanical Performance of Bridge Rotary Structure. *Buildings*. 2024. 14(12). Article no. 3905. DOI: 10.3390/buildings14123905
18. Nie, F., Zhao, L., Zhang, D., Wang, H. Fine analysis and size optimization of spherical hinge in swivel construction, *Proceedings of the Institution of Civil Engineers – Structures and Buildings*. 2025. 178(3). Pp. 312–320. DOI: 10.1680/jstbu.24.00121
19. Shi, X., Liu, Z., Guo, Z., Cai, C.S., Jiang, C. Investigation on contact stress calculation method of spherical hinge structures for swivel construction, *Structures*. 2024. 69. Article no. 107290. DOI: 10.1016/j.istruc.2024.107290
20. Zhao, H. Research on mechanical properties of steel spherical hinge of asymmetric rotation constructed long-span cable-stayed bridge. *Industrial Construction*. 2021. 51. Pp. 116–121.
21. Huang, S., Yuan, Z., Tang, Y. Accurate Calculation Method and Verification for Friction Force of the Spherical Hinge Interface in Bridge Horizontal Rotation Construction. *China Journal of Highway and Transport*. 2021. 34(9). Pp. 231–241.
22. Shanghai, L. Construction Group Co. Technical regulations for the construction of bridge horizontal rotation method (in chinese). Shanghai Housing and Urban-Rural Construction Management Committee, 2016.
23. Peng, Y. *Elastic Mechanics* (in chinese). Beijing Science Press, 2015.
24. Popov, V.L. *Contact Mechanics and Friction: Physical Principles and Applications*. Springer. Berlin. Heidelberg, 2017. 30 p. DOI: 10.1007/978-3-662-53081-8
25. Johnson, K.L. *Contact Mechanics*. *Proceedings of the Institution of Mechanical Engineers. Part J: Journal of Engineering Tribology*. 2009. 223. Pp. 254–254.
26. Huang, S., Tang, Y., Yuan, Z., Huang, Y., Hu, J. Contact surface stress analysis and optimization in rotating superstructures. *Journal of Harbin Engineering University*. 2020. 41. Pp. 1790–1796.
27. Popp, A. *Mortar Methods for Computational Contact Mechanics and General Interface Problems: Thesis*. Munich, 2012. 236 p.

Information about the authors:

Feng Nie,

E-mail: 1007159549@qq.com

Xuhui Zhou,

E-mail: 251357091@qq.com

Huili Wang,

E-mail: wanghuili@dlut.edu.cn

Chenbo Zhang,

E-mail: 18636289345@163.com

Received 18.01.2025. Approved after reviewing 30.07.2025. Accepted 03.08.2025.